ISCI, Volume *19*

Supplemental Information

Phototactic Flocking of Photochemical Micromotors

Fangzhi Mou, Jianhua Zhang, Zhen Wu, Sinan Du, Zexin Zhang, Leilei Xu, and Jianguo Guan

Supplemental Figures

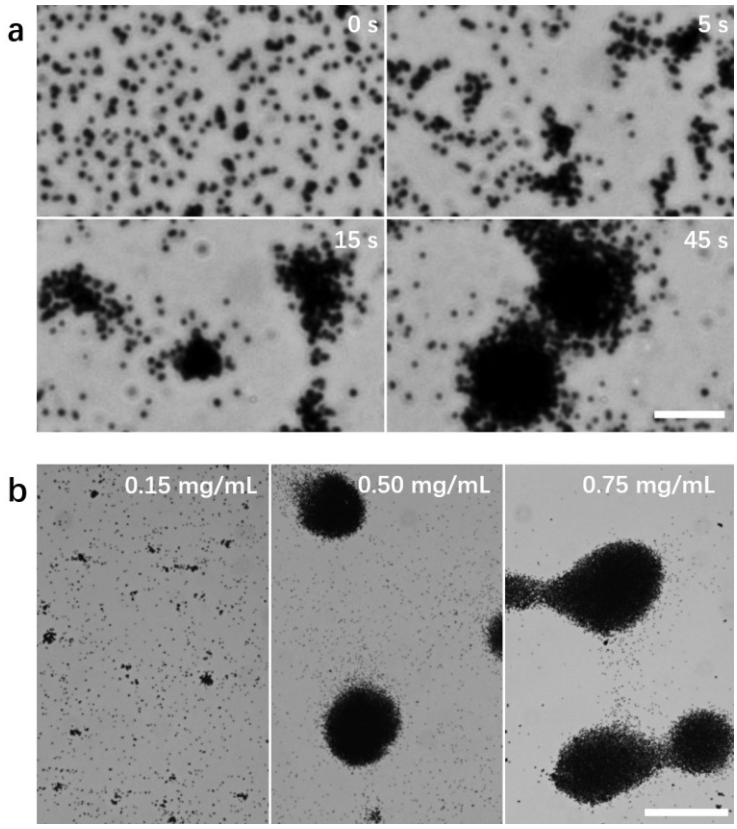

Figure S1. The clustering behaviors of the dispersed TiO2 micromotors. (a) The clustering process of the TiO2 micromotors over time. Images are taken from Video S1. Scale bar: 20 μm. Well-dispersed particles would gather into small flocks at first, and then they further grow into large flocks by absorbing neighboring particles or small flocks. (b) The formed TiO2 micromotor flocks at different Cp of 0.15, 0.5 and 0.75 mg/ml in water with 0.25 wt.% H2O2. Scale bar: 100 μm. Related to Figure 1.

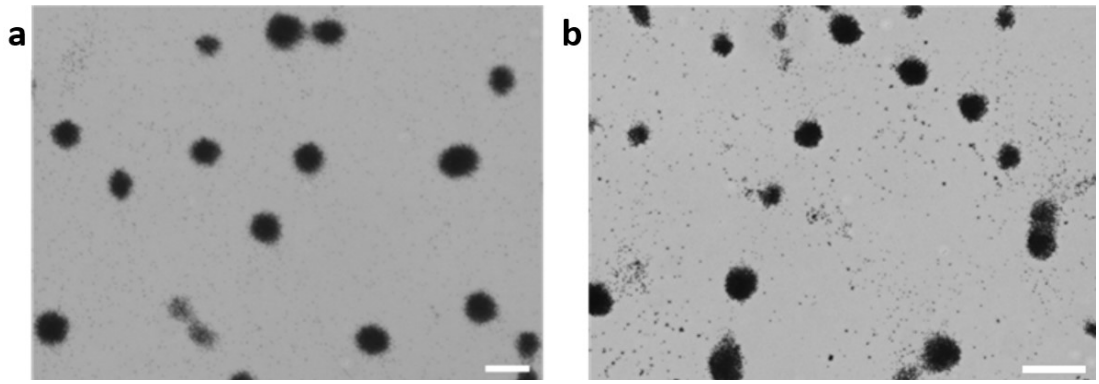

Figure S2. Flocks formed in pure water under natural light and in dark. (a) The flocks of TiO_2 micromotors formed in pure water. (b) The flocks of TiO_2 micromotors formed in 0.25 wt.% H_2O_2 solution in dark. Scale bars: 50 μm. Related to Figure 1.

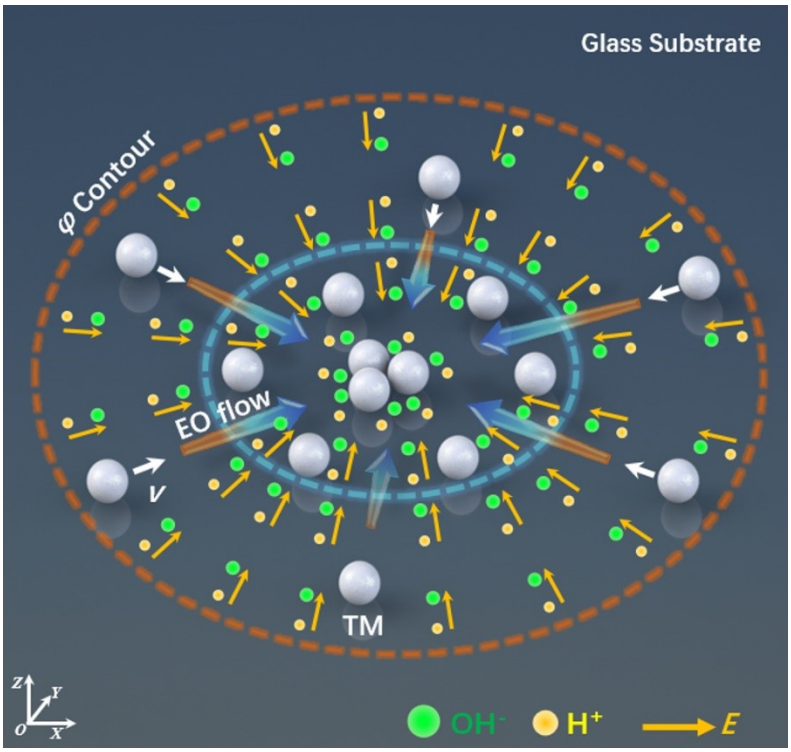

Figure S3. Clustering mechanism. The schematic illustration of the clustering of TiO_2 micromotors (TM) along with the electroosmotic flow (EO flow) under electrolyte diffusiophoresis. Related to Figure 1.

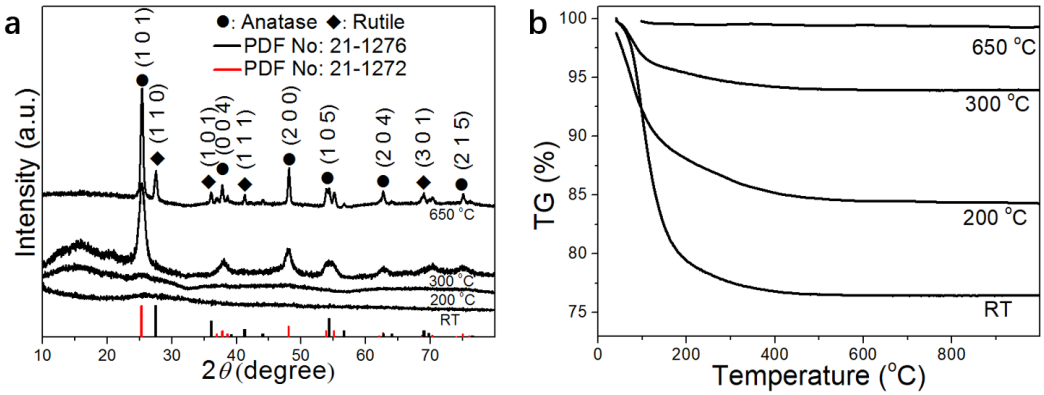

Figure S4. Characterization of TiO_2 micromotors obtained at different temperature. (a) XRD patterns and (b) TG analysis of the TiO_2 micromotors before calcination (RT) and those calcined at 200, 300 and 650 °C, respectively. Related to Figure 1.

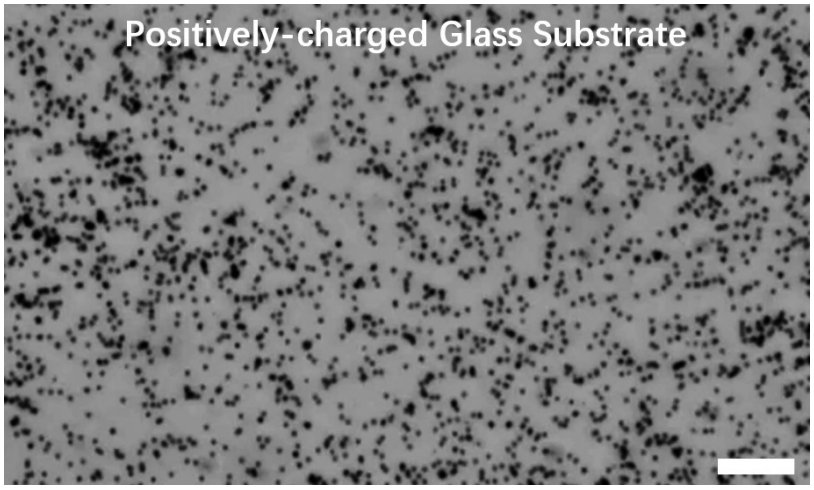

Figure S5. The TiO2 micromotors on a positively-charged glass substrate in the medium. Scale bar: 50 μm. Related to Figure 1.

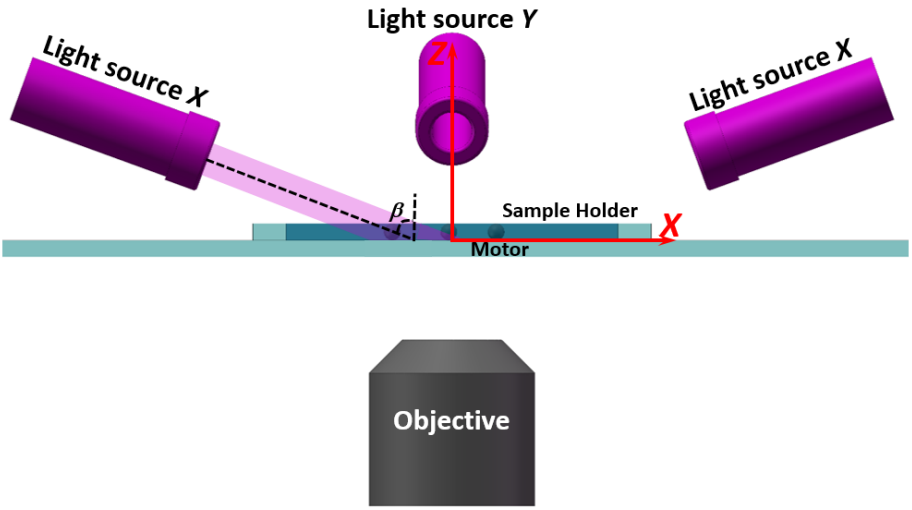

Figure S6. Schematic diagram of the experimental setup for the light irradiation. The coordinate is set up as demonstrated, Y axis points into the screen, light irradiators X and Y control the motion at X, Y directions respectively. For the convenience of operation, the light sources were set up to have an angle β with Z axis. Related to Figure 2.

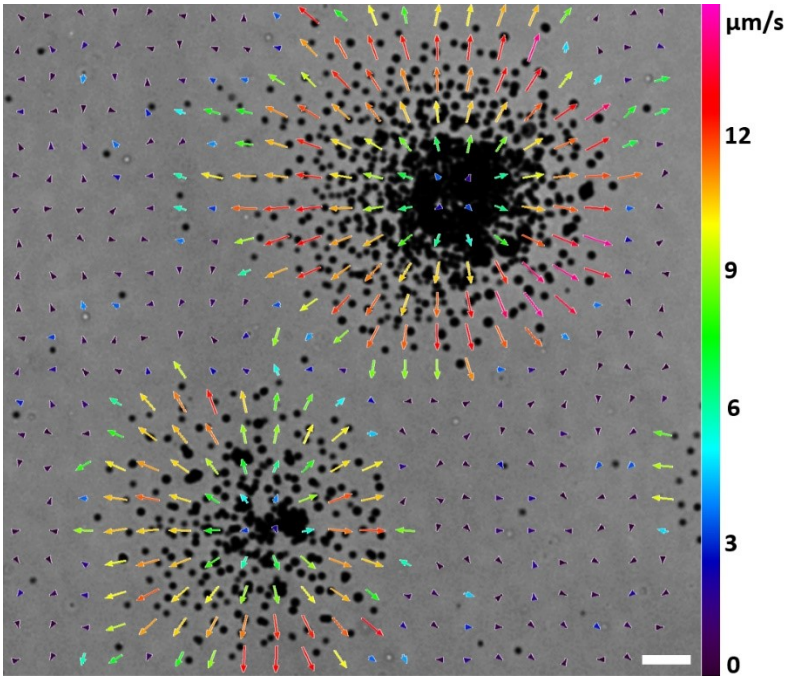

Figure S7. Instantaneous velocity vectors of the TiO_2 micromotors in two flocks under UV_Z irradiation. Related to Figure 2.

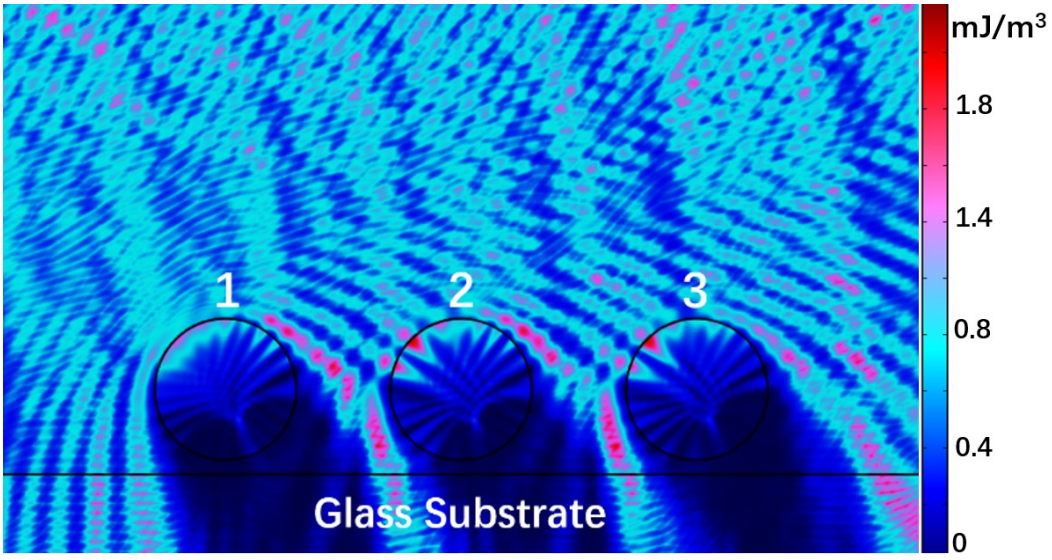

Figure S8. Numerical simulation of light intensity in micromotors. The simulated time-averaged light energy density in TiO_2 micromotor 1, 2 and 3 with an interparticle distance of 3 μm. Related to Figure 2.

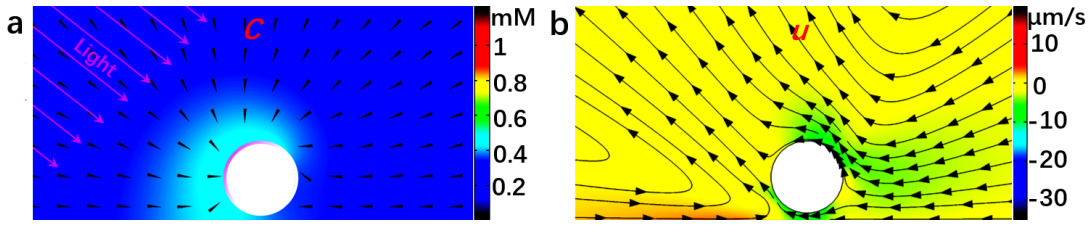

Figure S9. (a) Steady-state distribution of O_2 concentration (C) around a TiO_2 micromotor, in which the black triangles represent the gradient (∇C) of O_2 concentration. Purple arrows and curves represent the direction of incident UV light and the illuminated surfaces of the micromotors, respectively. (b) The simulated velocity in the X direction (u) and the streamlines (black curves) of the hydrodynamic flow induced by ∇C along the surface of the particles. Related to Figure 2.

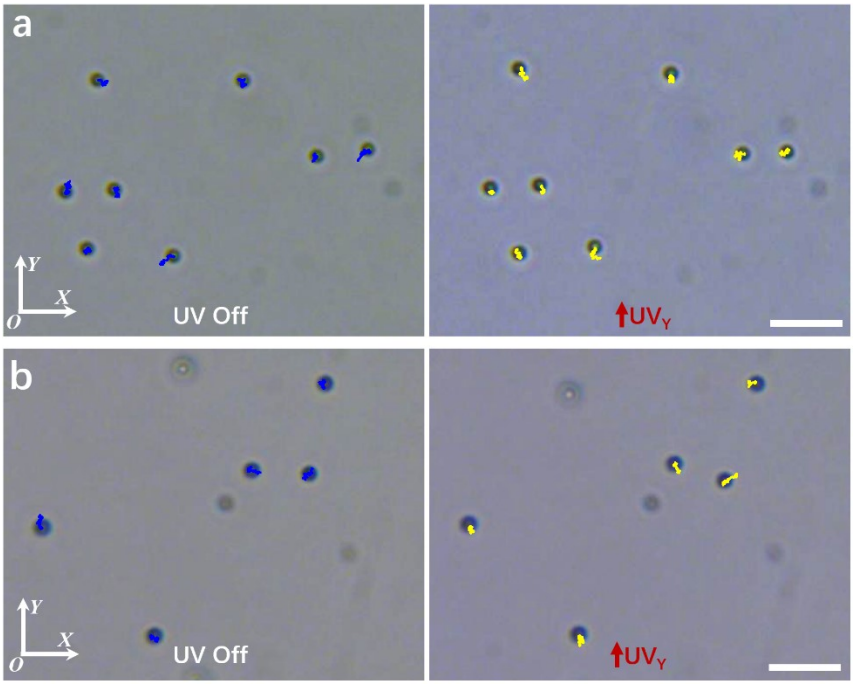

Figure S10. The motions of the passive (a) SiO2 and (b) PS microparticles when UV_Y is off and on, respectively. Images are taken from Video S5. Scale bar: 10 μm. Related to Figure 2.

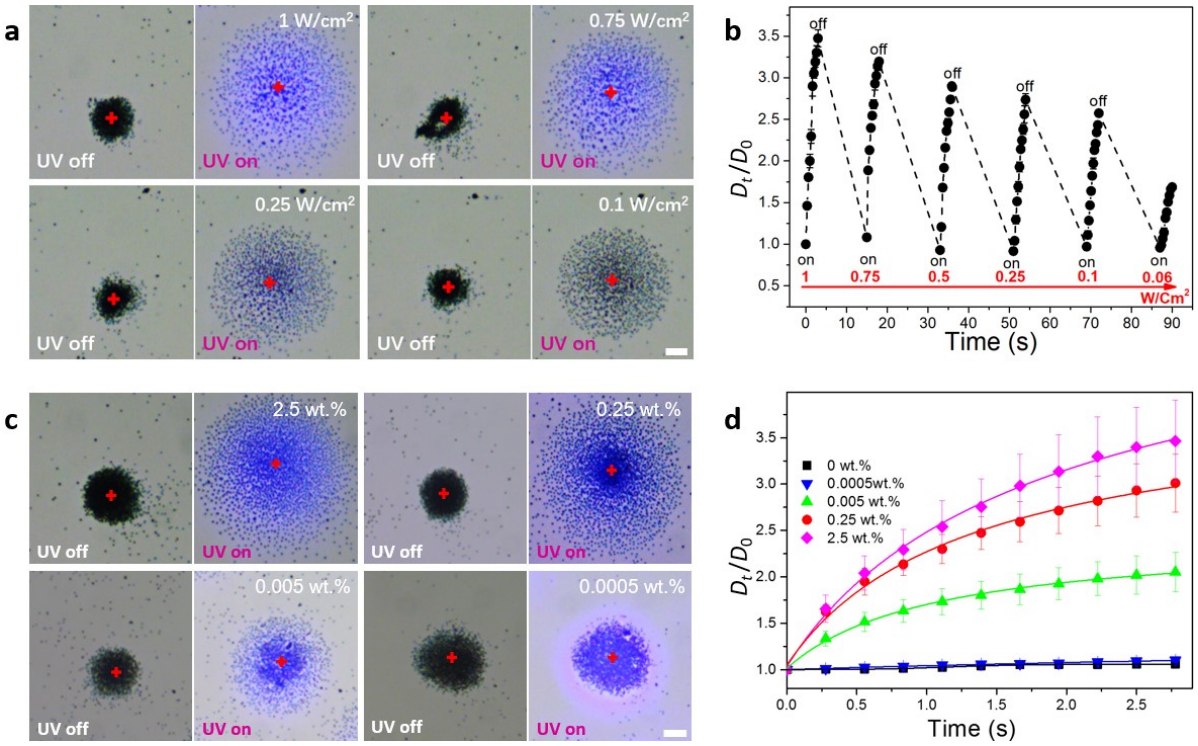

Figure S11. Phototaxis of the micromotor flocks at different UV intensity and fuel concentration. (a) Representative snapshots of the micromotor flock without and with UV irradiation at different light intensities, and (b) the normalized size (D_t/D_0) variation of the flock at different light intensities. (c) Representative snapshots of the micromotor flock without and with UV irradiation at different fuel concentration, and (d) the corresponding D_t/D_0 versus irradiation time. Scale bars: 20 μm. Related to Figure 3.

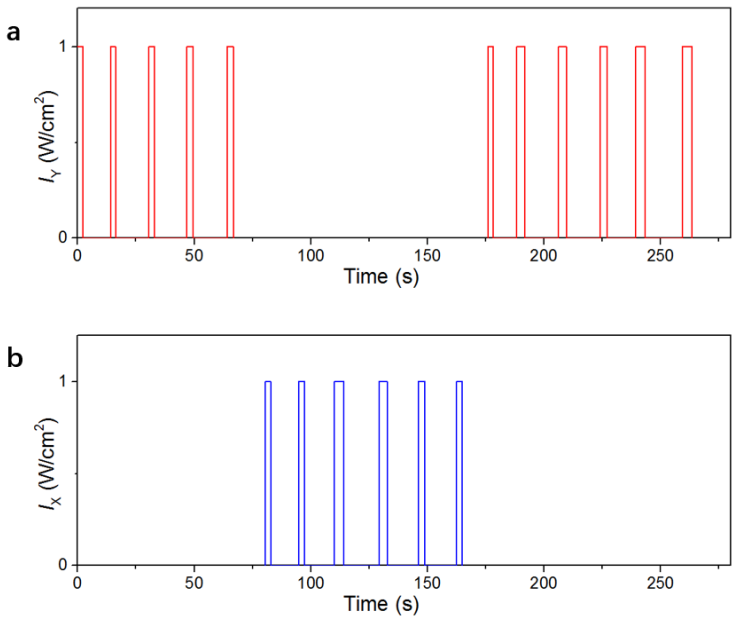

Figure S12. The on-off repeating cycles of UV irradiation. (a) The on-off repeating cycles of UV_Y for the navigation of the phototactic flock in the Y direction. (b) The on-off repeating cycles of UV_X for the navigation of the phototactic flock in the X direction. Related to Figure 3.

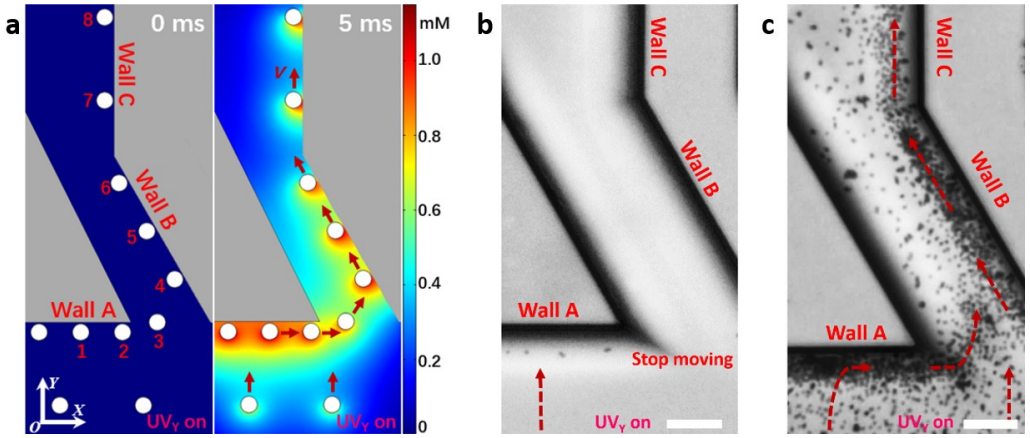

Figure S13. Interactions between individual micromotors and obstacle walls. (a) Numerical simulation of the distribution of the photocatalytically generated O_2 around the micromotors near obstacle walls with different angles (ϑ) to their phototactic motion axis (Y direction). Interacting micromotors could easily move along Wall A (ϑ = 90°), Wall B (ϑ = 60°) and Wall C (ϑ = 0°) due to the desired O_2 gradient across the micromotors (Micromotor 1-8) along the walls. (b) The trapped single motors near Wall A under UV_Y irradiation. (c) The flocking of the micromotors along obstacle walls under UV_Y irradiation. Scale bars: 20 μm. Related to Figure 4.

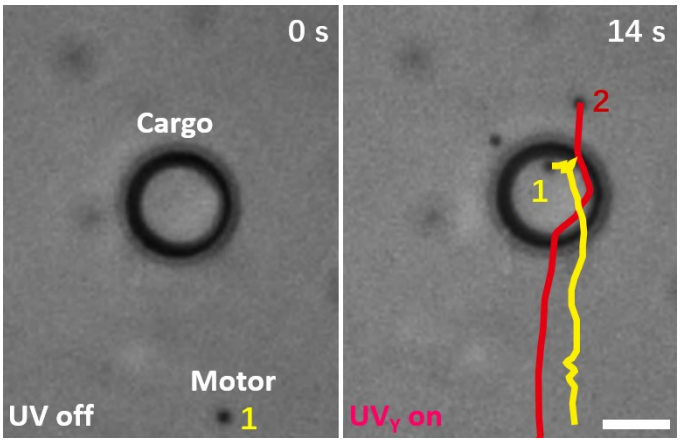

Figure S14. Cargo transport by single micromotors. Time-lapse optical microscopic images showing that single TiO_2 micromotors (motor 1 and 2) fail to move a large cargo (10 μm in size) due to its small size and weak driving forces. Yellow and red curves are trajectories of motor 1 and 2 under UV irradiation, respectively. Scale bar: 5 μm. Related to Figure 5.

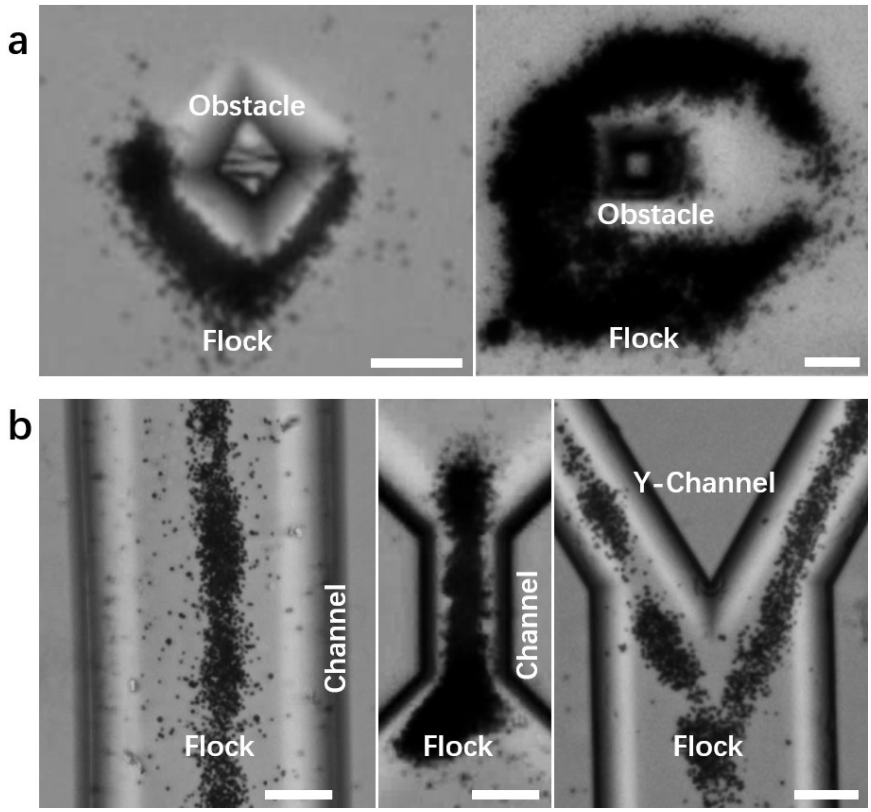

Figure S15. Collective patterns of the micromotor flocks in local microenvironments. (a) V-shaped and C-shaped flocks are formed if they embrace rhombus and square obstacles, respectively. (b) Wire-like, dumbbell, and Y-shaped micromotor flocks are formed in straight, flared and Y-shaped microchannels, respectively. Scale bars: 20 μm. Related to Figure 4.

Transparent Methods

Synthesis of TiO_2 micromotors. Spherical anatase TiO_2 microparticles with rich hydroxyl groups were fabricated as individual micromotors (Chen et al., 2017b). At first, the hydrous TiO_2 microparticles with a diameter of 1.2 μm were synthesized referring to the previous method. Then, the hydrous TiO_2 microparticles were calcined at 300 °C for 2 h to crystalize the microparticles while maintaining their high C_{OH}. Anatase TiO_2 microparticles with different C_{OH} were also fabricated by calcining the hydrous TiO_2 microparticles at 200 and 650 °C for 2 h, respectively. Those microparticles obtained at 650 °C were further treated by the alkaline hydrogen peroxide solution with 8 M NaOH and 0.1 M H_2O_2 to increase their C_{OH} (Wu et al., 2016).

Characterization. Scanning electron microscopy (SEM) images were obtained by Hitachi S-4800 Field-emission SEM (Japan). The Zeta potential of the micromotors was measured by Malvern Zetasizer Nano Z (Britain). The X-ray diffraction (XRD) patterns of the samples were recorded using a Rigaku D/Max-2000 diffractometer equipped with a Cu K radiation source (λ=0.15418 nm). Thermogravity-differentiatial scanning calorimeter (TG-DSC) analysis was carried out on a NETZSEC STA-449C thermal analyzer (Germany). The quantitative elementary analysis of hydrogen was measured by CHNS/O element analyzer (Vario EL cube, Germany). The hydroxyl group content in the TiO_2 micromotors is calculated from the curves of TG weight loss and quantitative elementary analysis.

Spontaneous clustering and phototactic flocking of the TiO_2 micromotors. A 100 μL suspension of the TiO_2 micromotors was dropped onto a glass slide (Citotest 1A5107), followed by adding 100 μL of the 0.5 wt.% H_2O_2 fuel solution. The concentration of the micromotors in the suspension was adjusted to 0.15, 0.35, 0.5 and 0.75 mg ml^{-1} to observe their clustering behaviors, respectively. Clustering behaviors of the micromotors in the medium without H_2O_2, in dark and on a positive-charge modified glass slide (Citoglas 188105W) were also investigated. Four lamps with a wavelength of 365 nm (SZ Lamplic Technology) were set above the substrate along with two orthogonal directions (see Figure S6), the incident angles (β) were set to be 45°. The four UV lamps (SZ Lamplic Technology, China) with maximum I of 1 W cm^{-2} were switched on and off serially according to the pre-designed program. The motions of the micromotor flock under the navigation of light were observed and recorded at room temperature by an inverted optical microscope (Leica DMI 3000 M). Videos were analyzed by using ImageJ and Video Spot Tracker V08.01 software. The velocity of the flock was determined by calculating the displacement of centroid of flocks per second under light irradiation.

Particle image velocimetry analysis. The velocity field of the micromotor flocks was quantitatively determined by micro-particle imaging velocimetry (μPIV) (Lindken et al., 2009), which provides velocity data at the micrometer scale. Here the μPIV analysis was performed using an in-house computer program written in Interactive Data Language (IDL, Exelis Visual Information Solutions). Briefly, two sequential digital images were taken by a bright-field microscope. The images were divided into small regions as interrogation windows, and then the local mean displacement of each point contained in the interrogation window was calculated by a two-dimensional cross-correlation algorithm. The corresponding velocity of each point was calculated by dividing the displacement vector by the time interval between the two images. Unlike conventional PIV measure where tracer particles are added for the visualization of motions, here the micromotors themselves act as tracers.

Quantitative Detection of the flux of O_2 molecules from TiO_2 micromotors. A 10 mL aqueous suspension of TiO_2 micromotors (0.07 mg mL^{-1}) and H_2O_2 (0.25 wt.%) was put into a 10 mL beaker mounted with the probe of dissolved oxygen meter (Jenco 9173R, USA). A UV-LED light source (SZ Lamplic Technology, China) with a wavelength of 365 nm was set below the beaker. The concentration of the dissolved oxygen was measured when the UV light (I = 1 W cm^{-2}) was

turning on and off repeatedly. The concentration of the dissolved oxygen in a solution only with H_2O_2 (0.25 wt.%) was also measured by taking the same procedures. The flux of O_2 molecules ($\boldsymbol{J}_{O_2}$) from the illuminated surface of the micromotors was calculated according to the following equation.

$$\boldsymbol{J}_{O_2} = \frac{C_t - C_0}{NS_p t} = \frac{2\pi r\rho(C_t - C_0)}{3C_P V t}$$

Here, C_0 is the concentration of the dissolved oxygen in the aqueous suspension before UV irradiation, and C_t is that at time of t under UV irradiation, in which C_t is obtained by deducting the increased O_2 concentration at t of the H_2O_2 (0.25 wt.%) solution under UV irradiation. N is the number of TiO_2 micromotors in unit volume. S_p and r are the surface area and radius of a TiO_2 micromotor. C_p is the concentration of TiO_2 micromotors in the aqueous suspension, and V is the volume of the aqueous suspension.

Numerical simulation.

a. Governing equations

Electrolyte diffusiophoretic interactions between TiO_2 micromotors

When the TiO_2 micromotors with rich hydroxyl groups are dispersed in water, they simultaneously secrete H^+ ions from surface acidic bridging hydroxyls (pK_a = 2.9) and OH^- ions from basic terminal hydroxyls (pK_b = 1.3), respectively. The distribution of H^+ and OH^- is determined by the ion flux ($\boldsymbol{J}_i$), diffusion, convection and migration of ions (Equation 1), and it is solved with the conservation equation (Equation 2) at steady state.

$$\boldsymbol{J}_i = \boldsymbol{u}c_i - D_i\boldsymbol{\nabla}c_i - \frac{z_i F D_i c_i \boldsymbol{\nabla}\varphi}{\mathrm{RT}} \quad (1)$$

$$\boldsymbol{\nabla}\cdot\boldsymbol{J}_i = \mathbf{0} = \boldsymbol{u}\cdot\boldsymbol{\nabla}c_i - D_i\boldsymbol{\nabla}^2 c_i - \frac{z_i F D_i \boldsymbol{\nabla}\cdot(c_i\boldsymbol{\nabla}\varphi)}{\mathrm{RT}} \quad (2)$$

Where $\boldsymbol{u}$ is the fluid velocity, F is the Faraday constant, φ is the electrostatic potential, R is the gas constant, T is the absolute temperature, and c_i, D_i, z_i are the concentration, diffusion coefficient, and charge of species i (H^+ or OH^-), respectively.

The electric potential (φ) in Equation 1 is calculated using the Poisson equation,

$$-\varepsilon_0\varepsilon_r\boldsymbol{\nabla}^2\varphi = \rho_e = F(z_+c_+ + z_-c_-) \quad (3)$$

where ρ_e is the volumetric charge density, z_+ and z_- are the charges of the cations and the anions, c_+ and c_- are the concentrations of the cations and the anions, ε_0 is the permittivity of the vacuum, and ε_r is the relative permittivity of the fluid media, respectively.

The inertial effect is neglected in the present study because of a very small Reynolds number. Thus, the flow field is governed by the Stokes equations,

$$-\nabla p + \mu\nabla^2\boldsymbol{u} = 0 \quad (4)$$

and the continuity equation for the incompressible fluid,

$$\nabla\cdot\boldsymbol{u} = 0 \quad (5)$$

In these equations, $\boldsymbol{u}$ is the fluid velocity vector, and p is the pressure. The initial values of the flow velocity and the pressure are all zero. The electroosmotic flow boundary conditions are as following:

On the particle surface, $\boldsymbol{u} = \frac{\varepsilon_0\varepsilon_r\zeta_p}{\mu}(\mathbf{I} - \mathbf{nn})\cdot\nabla\varphi$ (6)

On the substrate surface, $\boldsymbol{u} = \frac{\varepsilon_0\varepsilon_r\zeta_w}{\mu}(\mathbf{I} - \mathbf{nn})\cdot\nabla\varphi$ (7)

In these equations, ζ_p and ζ_w are the Zeta potential of the TiO_2 micromotors and the wall (glass substrate), respectively. The quantity $(\mathbf{I} - \mathbf{nn})$ defines the electric field tangential to the charged surface, with $\mathbf{I}$ denoting the second-order unit tensor.

Nonelectrolyte diffusiophoretic interactions between TiO_2 micromotors under UV irradiation

Under UV irradiation, a flux of O_2 molecules is induced on the illuminated surfaces of the TiO_2 micromotors due to the

photocatalytic decomposition of H_2O_2. The distribution of O_2 molecules is governed by the O_2 flux ($\boldsymbol{J}_{O_2}$), diffusion and convection (Equation 8), and it is solved with the conservation equation (Equation 9) at steady state.

$$\boldsymbol{J}_{O_2} = \boldsymbol{u}c_{O_2} - D_{O_2}\boldsymbol{\nabla}c_{O_2} \quad (8)$$

$$\boldsymbol{\nabla}\cdot\boldsymbol{J}_{O_2} = \boldsymbol{0} = \boldsymbol{u}\cdot\boldsymbol{\nabla}c_{O_2} - D_{O_2}\boldsymbol{\nabla}^2 c_{O_2} \quad (9)$$

Where c_{O_2} and D_{O_2} are the concentration and diffusion coefficient of O_2 molecules in water, respectively. Also, the inertial effect is neglected, the fluid is considered to be incompressible, and initial values of the flow velocity and the pressure are all zero in the present study. The boundary conditions of the chemiosmotic slip are as following:

On the particle surface, $\boldsymbol{u} = -b_p(\mathbf{I} - \mathbf{nn})\cdot\nabla c_{O_2}$ (10)

On the substrate surface, $\boldsymbol{u} = -b_w(\mathbf{I} - \mathbf{nn})\cdot\nabla c_{O_2}$ (11)

In these equations, b_p and b_w are surface mobility of the TiO_2 micromotors and the glass substrate that encapsulate the molecular details of the interaction between the solute (O_2 molecules) and the surface.

b. Parameter setting in COMSOL model

The simulations were performed by using diffusions, electrostatics and creeping flow modules of COMSOL Multiphysics software. For the numerical simulation of the local *E* generated by the different diffusivities of the secreted H^+ and OH^- and the electroosmotic flow induced by *E*, the simulation model is built up by placing three TiO_2 micromotors on a glass substrate (100 μm in width), which is immersed in the bottom of 0.01 mm^2 square space which is filled with water. The release rate and diffusion coefficients (*D*) of H^+ and OH^- are set to be 8.90×10^{-8} mol $m^{-2}\cdot s^{-1}$, 9.31×10^{-9} m^2 s^{-1} and 5.27×10^{-9} m^2 s^{-1}, respectively (Jang et al., 2016). Zeta potential (ζ) of the TiO_2 micromotors was measured to be -17 mV, and that of the glass substrate was set to be -85 mV (Duan et al., 2013), respectively. The bulk proton concentration was set to be 2.24×10^{-3} mol m^{-3}, the value for saturated water with ambient CO_2 at pH 5.65 (Jang et al., 2016). For the numerical simulation of the asymmetric O_2 concentration (*C*) distribution and chemiosmotic flow around three TiO_2 micromotors with an interparticle distance of 2 μm, and the flux (J_{O_2}) of O_2 molecules from the illuminated surface of the TiO_2 micromotor due to the photocatalytic H_2O_2 decomposition was measured to be 4.13×10^{-4} mol m^{-2} s^{-1}. The surface mobility over the particle surface (b_p) is deduced to be 8.50×10^{-11} m^5 mol^{-1} s^{-1} by parameter sweep in the simulation of the chemiosmotic flow velocity in *X*-axis (*u*) at the surface according to J_{O_2} and *v* (4.5 μm s^{-1}) of a single TiO_2 particle, and surface mobility over the substrate surface (b_w) is set to be $0.5b_p$ (Singh et al., 2018). The diffusion coefficient of O_2 molecules in water is 1.97×10^{-9} m^2 s^{-1} (Chen et al., 2017b).

Supplemental References

Jang, B., Wang, W., Wiget, S., Petruska, A.J., Chen, X., Hu, C., Hong, A., Folio, D., Ferreira, A., Pane, S., *et al.* (2016). Catalytic Locomotion of Core-Shell Nanowire Motors. ACS Nano *10*, 9983-9991.

Lindken, R., Rossi, M., Große, S., and Westerweel, J. (2009). Micro-Particle Image Velocimetry (μPIV): Recent developments, applications, and guidelines. Lab Chip *9*, 2551-2567.

Singh, D.P., Uspal, W.E., Popescu, M.N., Wilson, L.G., and Fischer, P. (2018). Photogravitactic Microswimmers. Adv. Funct. Mater. *28*, 1706660.